A COMPARISON OF SURFACE OBSERVATIONS AND ECHAM4−GCM EXPERIMENTS AND ITS RELEVANCE TO THE INDIRECT AEROSOL EFFECT

Beate G. Liepert and Ulrike Lohmann

Lamont−Doherty Earth Observatory Columbia University
Palisades, New York, U.S.A.
Email liepert@ldeo.columbia.edu

Department of Physics Dalhousie University
Halifax, Nova Scotia, Canada
Email Ulrike.Lohmann@dal.ca

ABSTRACT

The observations of solar irradiance at the surface, total cloud cover and precipitation rates have been used to evaluate aerosol−cloud−interactions in a GCM. Records from Germany and US were available for the time period from 1985 to 1990 and 1960 to 1990. The model used here is the ECHAM4 GCM run for a 5−year period with a fully coupled sulfur chemistry − cloud scheme (Lohmann and Feichter, 1997). We studied two experiments − one with an annual mean sulfate load of 0.36Tg S for the pre−industrial simulation and one with 1.05Tg S for the present day simulation.

Our goal was to indirectly confirm the existence of the indirect aerosol effect by finding indices for a better agreement of observations with the present day experiment compared to the pre−industrial experiment. We were able to draw such a conclusion only for the German data but not for the United States. The model correctly predicts the annual mean total cloud cover in Germany and the US, whereas global solar radiation is underestimated by 13W/m^2. This deficiency stems from cloudy conditions. Clouds are either optically too thick or the vertical distribution of clouds is erroneous. This is confirmed by the modeled overcast solar irradiance, which is 27W/m^2 lower than

observed whereas for the clear sky model the observations agree. Precipitation rates are underestimated by 42% in the United States. The seasonal cycle of the precipitation rate is incorrect in all US regions. The modeled cloud cover is too low over the Central United States in July and August and consequently the solar irradiance exceeds the observations during these months. The opposite occurs in winter when the model overestimates the cloud cover and thus underestimates solar irradiance. We suggest the non−seasonality of vegetation and soil parameters as possible causes for these deficiencies. The convective precipitation formation might also contribute to these discrepancies.

On the other hand, this drying out effect of the inner continent is not as pronounced in coastal regions and in particular, the comparisons for the German grid−box provide indications for the validity of the indirect aerosol effect. The modeled annual cloud cover and solar radiation cycles for the present day aerosol load are in better agreement with observations. Furthermore, the model shows an interesting shift from low cloud reduction to cirrus formation in spring as a consequence of the indirect aerosol effect, a result which is confirmed by observational data.

1. Introduction

Clouds are a major source of uncertainty in all global−climate−models (GCM) and therefore in the global climate change debate itself. The uncertainty is mainly related to the various scales involved in this problem. Aerosol − cloud processes act on the micro−physical scale and are constrained by large−scale parameters such as fractional cloud coverage, precipitation rate and cloud radiative properties that are crucial for any climate change prediction. In recent years major efforts have been made to measure and understand the physical key processes which link aerosol mass or number concentrations, cloud droplet number concentrations (CDNC) and cloud albedo and lifetime. The change in cloud optical properties due to anthropogenic emissions is called the "indirect aerosol effect". Ship track observations offer the most promising opportunity to study this indirect aerosol effect. Based on observational analyses several groups implemented aerosol − cloud schemes in their GCMs by empirically coupling sulfate aerosol mass or aerosol number concentrations with CDNC and cloud optical properties (Jones et al., 1994, Kogan et al., 1996, Chuang et al., 1997, Boucher and Lohmann, 1995). The predicted indirect aerosol forcing calculated by these authors range between −0.6 and $-1.6 W/m^2$ (Chuang et al., 1997) when natural aerosol load is compared to anthropogenic plus natural load.

In this study we try to assess the indirect effect of anthropogenic aerosols on climate by comparing relevant diagnostics of GCM experiments with surface climatologies. We do not directly analyze the cloud micro−physical processes involved. Rather we intend to evaluate the GCM itself with all dynamical features and feedback processes and all coupled processes of the hydrological cycle. The comparison with relevant observational

data provides an assessment of what is understood and what is missing in our effort to simulate the indirect aerosol effect.

The model experiments stem from the ECHAM4 GCM published by Lohmann and Feichter (1997). The climatologies used are total cloud coverage, precipitation and surface solar radiation.

2. Observations

The surface climatologies stem from two independent data sets. One database is the surface solar radiation network from the German Weather Service (DWD) that Liepert (1997) and Liepert and Kukla (1997) analyzed in detail. This package contains total broadband solar radiation recordings and fractional cloud cover observations from eight stations in Germany (Table 1). The second database is the national solar radiation database NSRDB of the United States (NREL, 1992). It also contains total broadband solar radiation recordings, fractional cloud coverage and additional precipitation rates. All data are available on an hourly basis. The chosen time interval from 1985 to 1989 fits the AMIP period (Atmospheric Model Intercomparison Project) of the ECHAM4 model forcing (Gates, 1992). The US records, however, are not coherent and exhibit major gaps between 1985 and 1989. Therefore, a selection of the most complete data sets (Table 1) was chosen and the time interval was expanded from 1960 to 1990. The data are checked for homogeneity by the providers (DWD and NCDC) and by the authors. The German radiation records are regarded as one of the most reliable worldwide. The accuracy of these observations is about $5 W/m^2$ and the accuracy of the US instrumentation lies around $15 W/m^2$ according to the World Radiation Monitoring Center (Ohmura et al.,

1998). The geographic distribution of the observational sites is shown in figure 1a and figure 1b.

TABLE 1. List of stations, geographic coordinates and type of observations.

	Location	Latitude, longitude	Solar irradiance, total cloud cover	Precipitation rate
GER				
1	Norderney	53.72N, 7.15E	yes	no
2	Hamburg	53.63N, 10.00E	yes	no
3	Braunschweig	52.30N, 10.45E	yes	no
4	Braunlage	51.72N, 10.53E	yes	no
5	Trier	49.75N, 6.67E	yes	no
6	Wuerzburg	49.80N, 9.90E	yes	no
7	Weihenstephan	48.40N, 11.73E	yes	no
8	Hohenpeissenberg	47.78N, 11.02E	yes	no
US				
1	Albuquerque	35.03N, 106.62W	yes	yes
2	Boise	43.57N, 116.22W	yes	yes
3	Boulder	40.00N, 105.25W	yes	yes
4	Burlington	44.47N, 73.15W	yes	yes
5	Burns	43.57N, 119.05W	yes	yes
6	Caribou	46.87N, 68.02W	yes	yes
7	Columbia	38.82N, 92.22W	yes	yes
8	Daytona Beach	29.17N, 81.05W	yes	yes
9	Dodge City	37.77N, 99.97W	yes	yes
10	El Paso	31.78N, 106.40W	yes	yes
11	Ely	39.27N, 114.83W	yes	yes
12	Eugene	44.12N, 123.22W	yes	yes
13	Fresno	36.77N, 119.72W	yes	yes
14	Grand Junction	39.12N, 108.52W	yes	yes
15	Lander	42.82N, 108.72W	yes	yes
16	Las Vegas	36.07N, 115.17W	yes	yes
17	Madison	43.12N, 89.32W	yes	yes
18	Montgomery	32.28N, 86.40W	yes	yes
19	Nashville	36.12N, 86.67W	yes	yes

20	Omaha	41.37N, 96.52W	yes	yes
21	Phoenix	33.42N, 112.17W	yes	yes
22	Pittsburgh	40.50N, 80.22W	yes	yes
23	Raleigh	35.87N, 78.77W	yes	yes
24	Salt Lake City	40.77N, 111.97W	yes	yes
25	Savannah	32.12N, 81.18W	yes	yes
26	Seattle	47.45N, 122.30W	yes	Yes
27	Sterling	38.95N, 77.43W	yes	Yes
28	Tallahassee	30.37N, 84.37W	yes	Yes

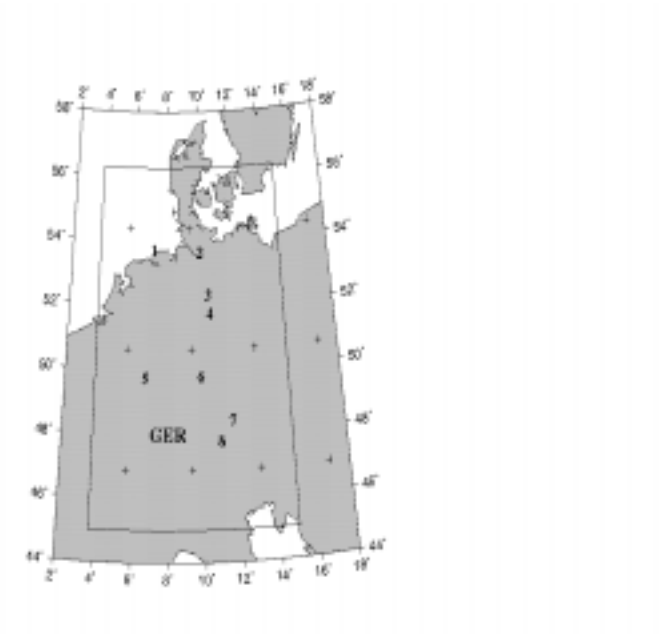

FIG. 1a. The map of Germany is shown. The numbers represent the German observational sites as listed in Table 1. Also shown is the model box "GER" and the model grid points "+".

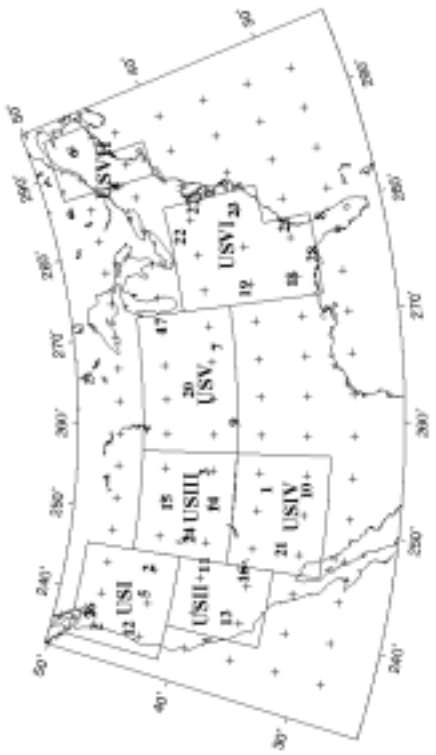

FIG. 1b. The map of the United States is shown. The numbers represent the US observational sites as listed in Table 1. The geographic distribution of the seven US model boxes and the model grid points "+" are also shown.

3. Model

3.1 Description

The modeled data stem from the ECHAM4 GCM developed at the Max Planck Institute for Meteorology in Hamburg, Germany. The ECHAM4 is a spectral model (T30) with a nominal resolution of 3.75 by 3.75 degrees. It is forced by observed sea surface temperature and ice coverage from the AMIP data set (Gates, 1992). The ECHAM4

cloud microphysics scheme (Lohmann and Roeckner, 1996) distinguishes between warm phase and ice phase processes and employs diagnostic schemes for rain and snow. The fractional cloud coverage is an empirical function of the relative humidity in the grid box (Sundqvist et al., 1989). Sulfate aerosol mass concentration is empirically linked to CDNC differently for maritime and continental clouds. The model version has a fully coupled sulfur chemistry scheme (Feichter et al., 1996). Here in this study, we refer to the experiment "COUPL" in Lohmann and Feichter (1997). Finally the radiation scheme is the typical two−stream approach used in most GCMs with two spectral bands in the shortwave. Cloud droplet effective radii are empirically related to the calculated volume radii with separate functions for maritime and continental clouds. The ice crystal effective radius is a function of ice water content.

Lohmann and Feichter (1997) describe the model experiment utilized in this analysis in detail. The five−year time interval from 1985 to 1989 has been chosen for the simulations. The indirect aerosol effect is derived as a difference from two experiments, one simulating pre−industrial (PI) and the other one present−day (PD) sulfate aerosol concentrations. The PI sulfate load is 0.36Tg S and the PD annual mean is 1.05Tg S.

3.2 Results

The selected model parameters for the comparison with observational data are total short−wave flux at the surface, precipitation rate and fractional cloud coverage. The difference at the surface between the solar irradiance from the two experiments PD and PI is shown in figure 2. The global mean difference and hence the mean surface indirect aerosol effect is $-1.9 W/m^2$. The precipitation is suppressed by 0.01mm/d and the total

cloud cover increases by 0.5% in the PD. The model predicts negative radiative effects mainly over the ocean ($-2.3 W/m^2$) and complex patterns over the continents with an average effect of $-0.7 W/m^2$. The land regions considered in this study show an average negative radiative effect of $-3 W/m^2$ for the US, with a positive effect for the mid−western region USIII and no effect for Central Europe GER and south−western United States USIV (Table 2). The fractional cloud cover increases only slightly by 1% with increasing CDNC. It also precipitates slightly more in the PD compared to the PI experiment over the US due to the increased cloud water. The regional distribution of the cloud and precipitation increase is similar (Table 3 and 4). In the following chapters we will interpret these calculated indirect aerosol effects by comparing both experiments with observational data.

TABLE 2. The surface solar irradiance from observations of eight regions in the United States and Germany (figure 1a and 1b) and two ECHAM4 GCM experiments (pre−industrial and present−day) are shown. Composites of annual means for each region, overall means for each cloud category and correlation coefficients of the monthly mean observations vs. pre−industrial experiment and the observations vs. present−day experiment are listed.

Global Solar Irradiation W/m²				
Category	Box	Observation	ECHAM4 Pre−industrial	ECHAM4 Present−day
All	***US I***	***175***	***156***	***151***
"	***US II***	***192***	***199***	***197***
"	***US III***	***183***	***182***	***186***
"	***US IV***	***223***	***229***	***229***
"	***US V***	***185***	***175***	***169***
"	***US VI***	***182***	***178***	***171***
"	***US VII***	***173***	***158***	***155***
"	***GER***	***118***	***111***	***111***
All	Mean	181	171	168
	Corr. Coef.		0.876 m 0.047	0.870 m 0.049
Clear	Mean	228	227	227
	Corr. Coef.		0.782 m 0.078	0.675 m 0.109
Overcast	Mean	112	89	85
	Corr. Coef.		0.637 m 0.119	0.582 m 0.133

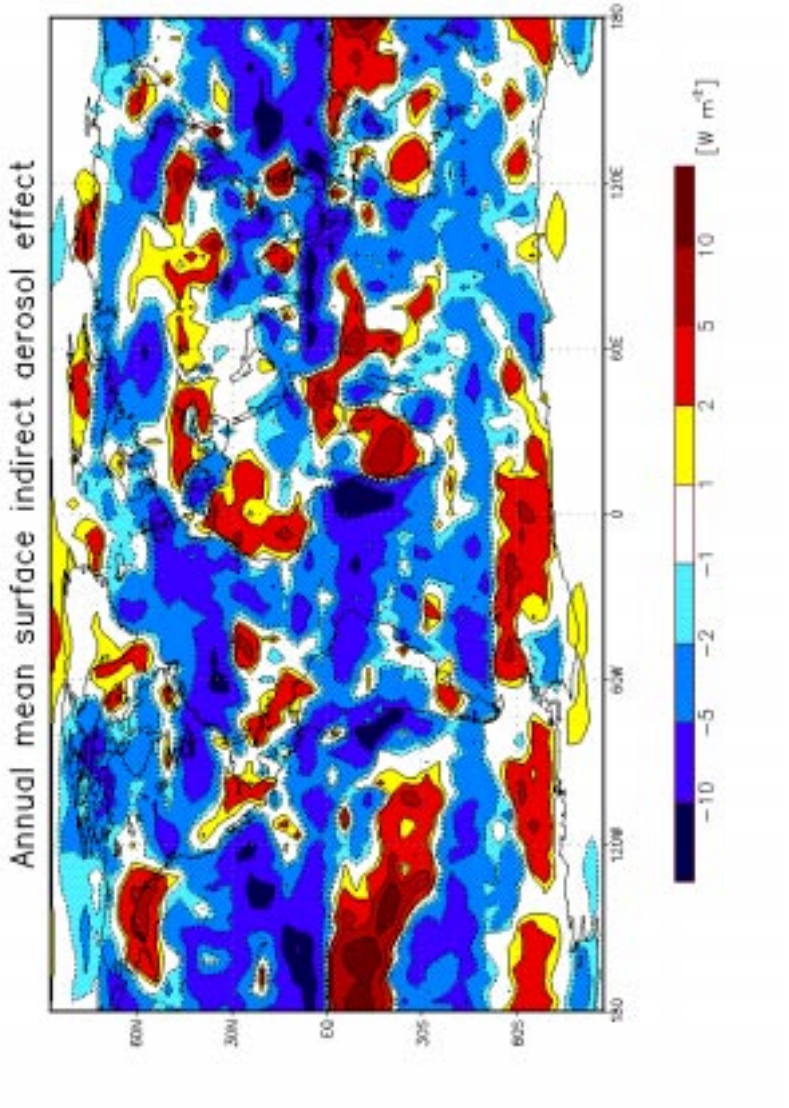
Annual mean surface indirect aerosol effect
60N
30N
EQ
30S
60S
180
120E
60E
0
60W
120W
180
−10
−5
−2
−1
1
2
5
10
[W m^{-2}]

FIG. 2. The annual mean surface indirect aerosol effect calculated as the difference in surface solar irradiance between the ECHAM4 GCM model experiment "present day" minus "pre−industrial".

4. Climatologies

Model − observation comparisons like this one, face the problem of defining the "same physical variables". Therefore special attention has been given to the data diagnostics in this study.

All modeled surface solar irradiance, precipitation rate and total cloud cover data are 12−hour means (twice a day), whereas the observational data are on an hourly basis (day and night). Therefore all observational records were recalculated to 12−hour means (0:01 to 12:00 and 12:01 to 24:00 local time) for each site.

Furthermore, the 12−hour means of the surface solar irradiance records for both, stations and grid−points, are grouped into three cloud categories with the 12−hour mean fractional cloud cover N_{12} for stations and grid−points as threshold criteria.

"All sky" solar irradiance	$0\% <= N_{12} <= 100\%$
"Clear sky" solar irradiance	$N_{12} <= 10\%$
"Overcast sky" solar irradiance	$N_{12} > 90\%$

Afterwards, the 12−hour mean solar irradiance data for "all", "clear" and "overcast" conditions are averaged into composites of 365(360 for the model) daily means and these composites finally into monthly means. The monthly composites for each site and each grid point are spatially averaged with seven regional means of the United States and one of Germany (see figures 1a and 1b). All other variables underwent the same sampling procedure. The regional monthly means of each variable are the basis of the statistical analyses performed in this study. The smallest region consists of three modeled and two

observed (USVII) and the largest region consists of eight modeled and eight observed data points (USVI).

5. Radiation Comparisons

In the scatter plot shown in figure 3a, the all sky monthly means of the modeled surface solar irradiance are plotted against the corresponding observed solar irradiance. All US and German data are included in this plot and additionally the regression lines for the two model runs PI and PD are drawn. (The regression is calculated with the method of least squares, with observations as the independent and model experiments as the dependent variable.) It can be seen in Table 2, that in general the model underestimates the averaged solar radiation by 10W/m^2 and this discrepancy increases to 13W/m^2 with higher aerosol loads. Nevertheless, the observed and the modeled data correlate quite well as indicated by the correlation coefficient in Table 2. (The correlation coefficient is calculated from the residuals of the seasonal cycle). The model underestimates the solar flux mostly below 200W/m^2 when compared to observations (see figure 3a). This result indicate deficiencies in the cloudy cases and thus in the cloud−scheme rather than in the different aerosol load. We will discuss the cloudiness in more detail in the next chapter.

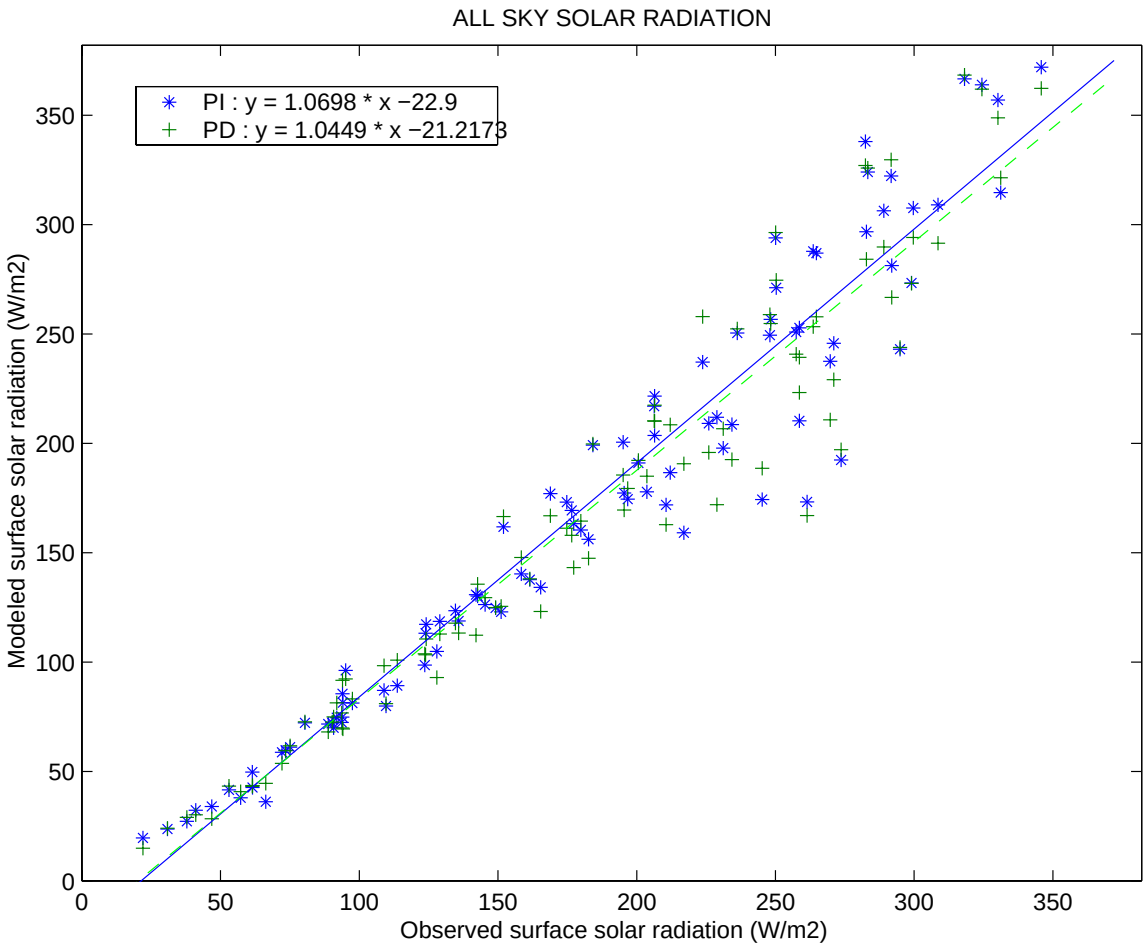

FIG. 3a. The scatter plot of the "all sky" monthly means of total solar irradiance at the surface is shown. The "PD" present−day experiment and the pre−industrial "PI" experiment are plotted against the observational data. The dashed line is the PD and the solid line is the PI regression.

The clear sky solar radiation climatologies are plotted in a scatter diagram in figure 3b. In the experimental set−up of the Lohmann and Feichter study (1997) the direct aerosol forcing is not included and a set of standard aerosols has been used in both experiments. Thus the slight differences in the two experiments stem only from cloud feedbacks on the model dynamics and internal variability. The overall mean modeled solar flux for clear

sky conditions equals almost the observed solar flux (Table 2). This was not the case in former versions of the ECHAM GCM (Wild and Liepert, 1998) and the improvements are due to changes in the radiation code, particularly the water vapor absorption (Roeckner et al., 1996). The clear sky correlation coefficient between observed and modeled data, however, is weaker than the correlation for all sky conditions though the 95% confidence interval is very broad. The weaker correlation is due to the general overestimation of the seasonal amplitude of the modeled clear sky flux, which has not improved since former ECHAM versions (see Wild and Liepert, 1998 for comparison).

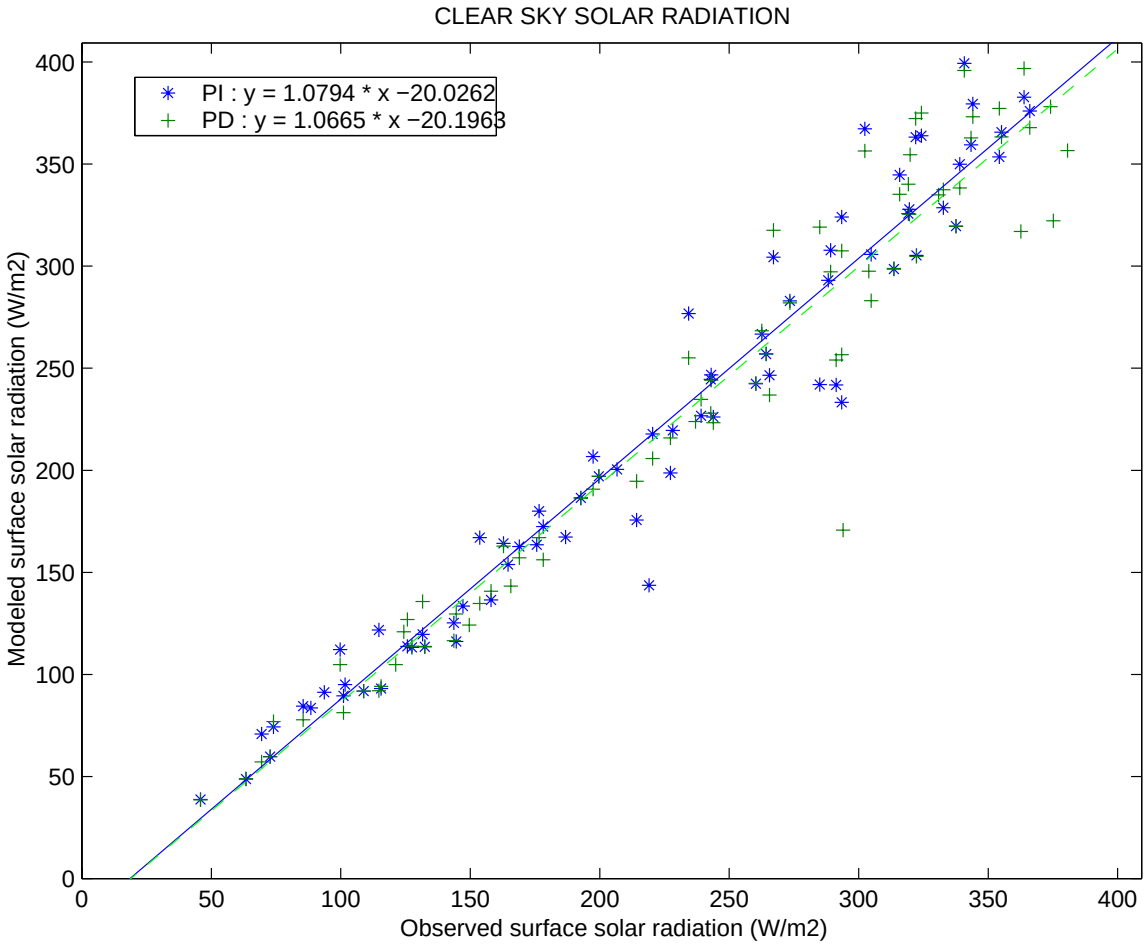

FIG. 3b. The scatter plot of the "clear sky" monthly means of total solar irradiance at the surface is shown. The "PD" present−day experiment and the pre−industrial "PI" experiment are plotted against the observational data. The dashed line is the PD and the solid line is the PI regression.

Finally, the solar radiation climatologies of the overcast skies are summarized in figure 3c. The model underestimates the solar fluxes for these overcast conditions by 23W/m^2 or 21% with PI aerosol concentrations (Table 2). The higher aerosol content in PD augments this tendency even more and the underestimation is 27 W/m^2. This is clearly higher than the all sky underestimation that includes the clear sky category with the correct prediction.

The modeled underestimation of the overcast solar radiation indicates either underestimated transmissivity of the model clouds, on an erroneous vertical distribution of the cloud layers like overestimated geometrically thickness of clouds or multi−layer clouds. The underestimation in the all sky category however could also be due to erroneous fractional cloud coverage itself, which will be discussed in the next chapter.

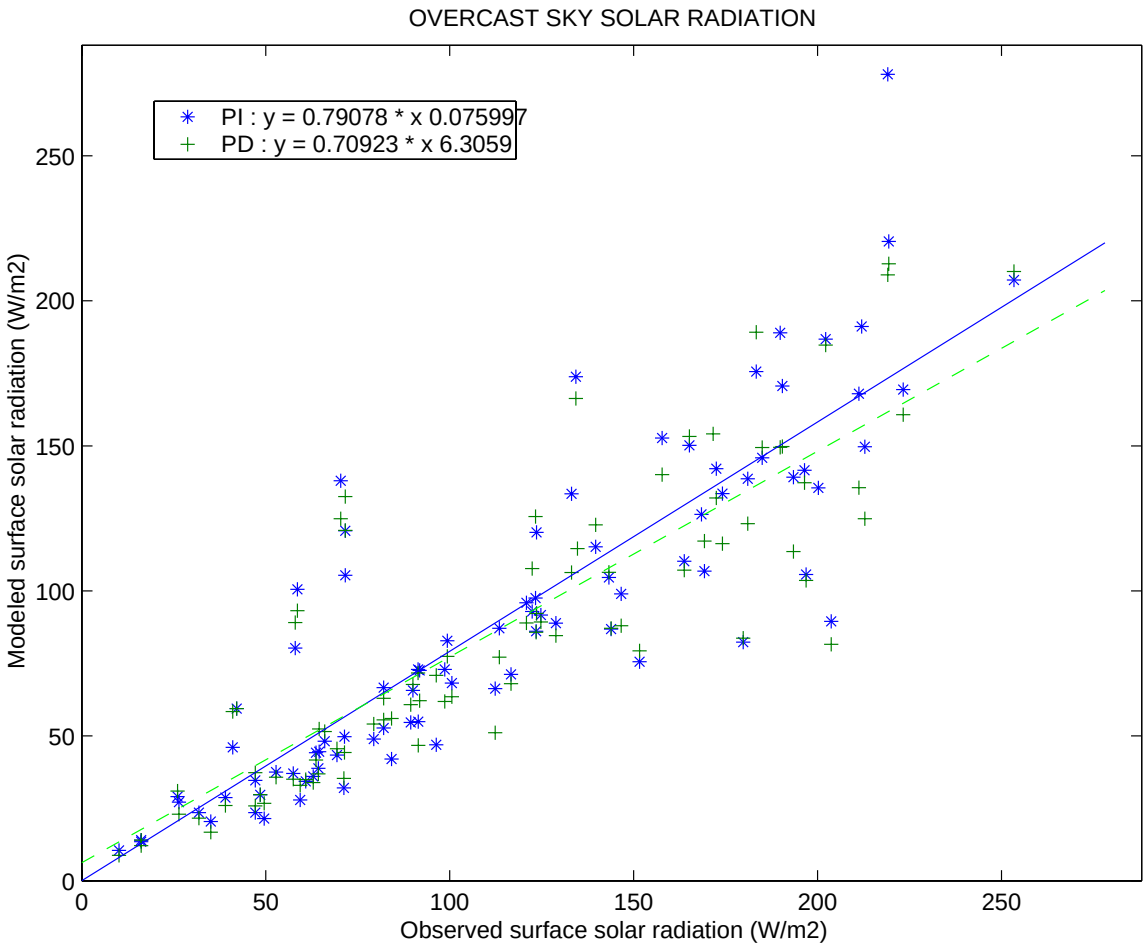

FIG. 3c. The scatter plot of the "overcast sky" monthly means of total solar irradiance at the surface is shown. The "PD" present−day experiment and the pre−industrial "PI" experiment are plotted against the observational data. The dashed line is the PD and the solid line is the PI regression.

6. Cloud and Precipitation Comparisons

Figure 4 shows the scatter plot of the modeled versus the observed fractional cloud coverage for the US and German data. The ECHAM4 cloud scheme predicts the mean cloud cover of 50% exactly as observed (see Table 3). The correlation between observed and predicted cloud coverage is rather strong as indicated by the correlation coefficients

(seasonal cycle is excluded) of 0.86 for PI and PD. However, ECHAM4 predicts months with cloud coverages below 20% whereas only one monthly mean below 20% was observed. One reason might be the visually taken cloud cover observations. On the other hand, the frequency of clear sky events is also highly overestimated by ECHAM4. If it were an observational problem, then the clear sky would be overestimated by an observer and not underestimated because of the difficulties to detect cirrus clouds. The model overestimation of the clear sky frequency is especially high in summer over the central United States. This effect, however, does not necessarily affect the annual mean cloud cover, whose prediction was in good agreement, because the cloud cover is already low at these months.

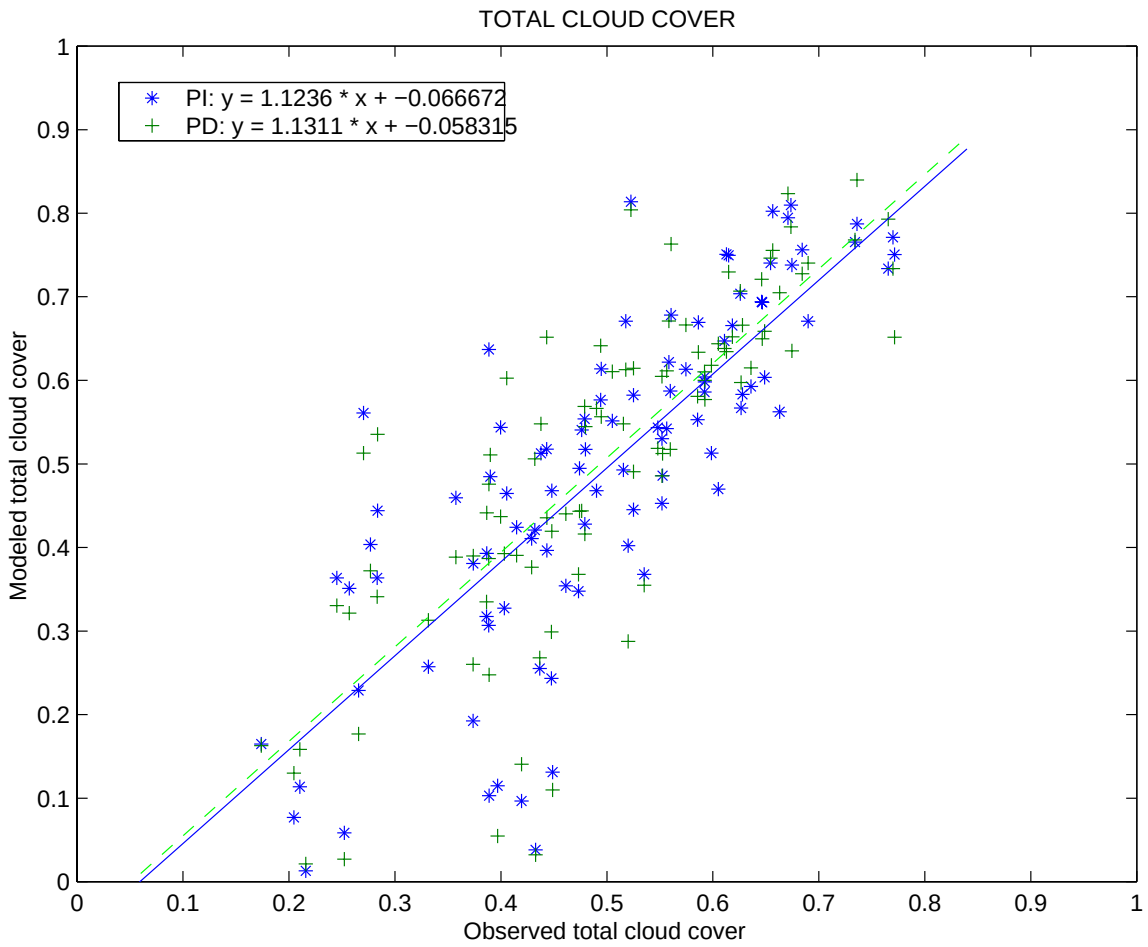

FIG. 4. The scatter plot of monthly means of fractional cloud cover is shown. The "PD" present−day experiment and the pre−industrial "PI" experiment are plotted against the observational data. The dashed line is the PD and the solid line is the PI regression.

TABLE 3. The fractional cloud cover from observations of eight regions in the United States and Germany (figure 1a and 1b) and two ECHAM4 GCM experiments (pre−industrial and present−day) are shown. Composites of annual means for each region, the overall mean and correlation coefficients of the monthly mean observations vs. pre−industrial experiment and observations vs. present−day experiment are listed.

Fractional Cloud Cover %			
Box	***Observation***	ECHAM4 Pre−industrial	ECHAM4 Present−day
US I	***57***	***55***	***59***
US II	***43***	***41***	***41***
US III	***49***	***46***	***47***

US IV	***37***	***33***	***32***
US V	***47***	***42***	***45***
US VI	***50***	***46***	***47***
US VII	***53***	***55***	***55***
GER	***66***	***64***	***66***
Mean	50	49	50
Corr. Coef.		0.856 m 0.053	0.860 m 0.052

The precipitation rates are shown in figure 5 but solely for the US stations. Precipitation is underestimated in all regions of the US (Table 4). Only monthly mean precipitation rates below 6mm/d are modeled whereas monthly means of up to 10mm/d were observed. The modeled overall mean precipitation rate is about 1.6mm/d lower than the observed using the present−day aerosol and thus underestimated by 42%. Only in three out of seven boxes is the modeled precipitation within the 30% range of the observations.

TABLE 4. The precipitation rate from observations of seven regions in the United States (figure 1a and 1b) and two ECHAM4 GCM experiments (pre−industrial and present−day) are shown. Composites of annual means for each region, the overall mean and correlation coefficients of the monthly mean observations vs. pre−industrial experiment and observation vs. present−day experiment are listed.

Precipitation Rate mm/d			
Box	***Observation***	ECHAM4 Pre−industrial	ECHAM4 Present−day
US I	3.5	2.6	2.7
US II	3.0	1.4	1.3
US III	2.5	1.6	1.8
US IV	3.3	1.1	1.1
US V	4.1	1.9	2.1
US VI	6.2	3.1	3.1
US VII	3.5	3.1	3.2
Mean	3.8	2.1	2.2
Corr. Coef.		0.525 m 0.146	0.538 m 0.143

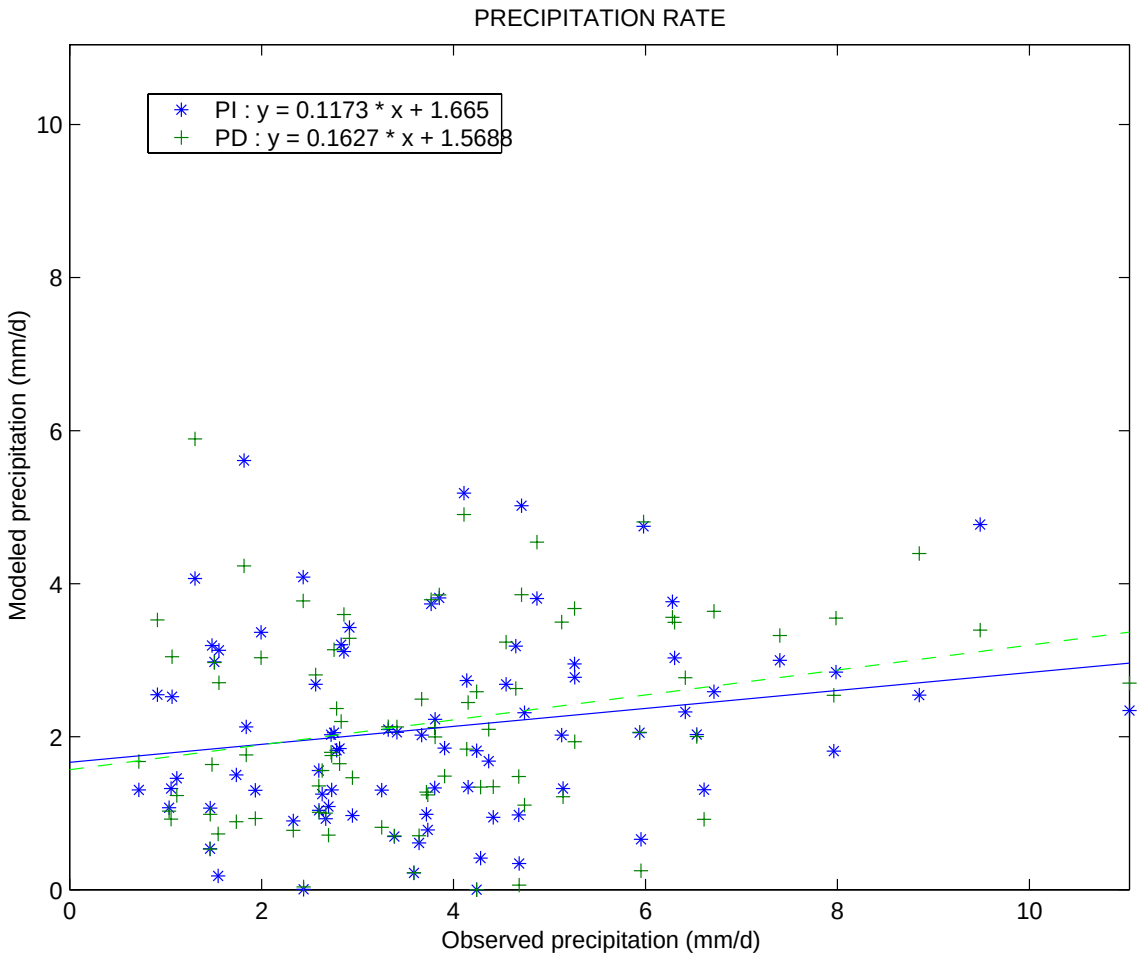

FIG. 5. The scatter plot of monthly means of precipitation rate is shown. The "PD" present−day experiment and the pre−industrial "PI" experiment are plotted against the observational data. The dashed line is the PD and the solid line is the PI regression.

Summarizing these results, the ECHAM4 cloud scheme predicts the right average cloud coverage but the cloud optical thickness is overestimated. Furthermore the model seems to underestimate precipitation rates. Incorrectly predicted cloud types might cause this discrepancy. This cloud bias might be caused either by large−scale circulation deficiencies in the model or deficiencies in the cloud scheme itself. A shift in frequency

from low level non−precipitating stratus to precipitating convective clouds with cirrus anvils would increase the precipitation while the total cloud cover would stay constant. The overall solar irradiance at the surface would increase because the lifetime of convective clouds is lower and the remaining cirrus clouds are optically much thinner. According to Roeckner et al. (1996) the main features of the circulation patterns over the United States are well captured with ECHAM4 when compared to ECMWF analysis. There are at least no obvious anomalies in the wind or pressure fields in the NH, which would explain the observed cloud anomalies. The following regional approach will provide more detailed information.

7. Regional Approach : Solar Radiation − Cloud Cover − Precipitation

Figure 6, 7 and 8 contain the mean annual composites of the "all sky" global solar radiation, total cloud coverage and precipitation rates for each region separately. The observed monthly means and the means of both model experiments are shown in one chart. The first seven plots represent the US regions and the last charts show Germany. For the solar irradiance shown in figure 6, the difference between the modeled seasonal cycles and the observations are more pronounced than the model experiments from each other. In general, the model overestimates the solar radiation in late summer and underestimates it in the winter months. The overestimation is emphasized when the regions are more continental and diminished nearer to the coast (either East or West Coast and the coast of the North Sea). The winter underestimation of solar irradiance seems more independent of the geographic location.

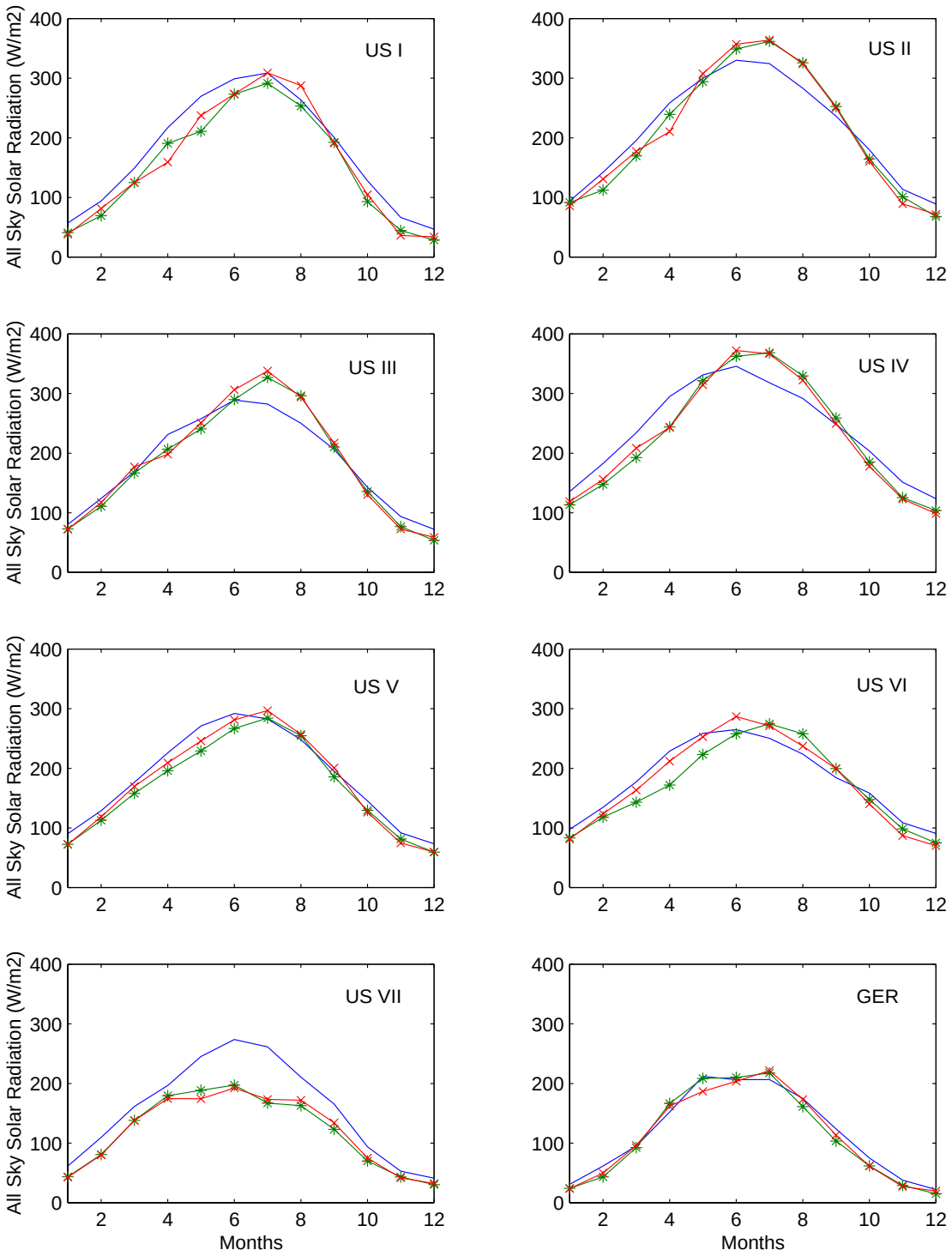

FIG. 6. The annual cycles of total solar irradiance at the surface for the eight regions as shown in figure 1a and 1b. The blue '__' line represents the observations, the green '*' the present−day "PD" and the red '+' the pre−industrial "PI" experiment.

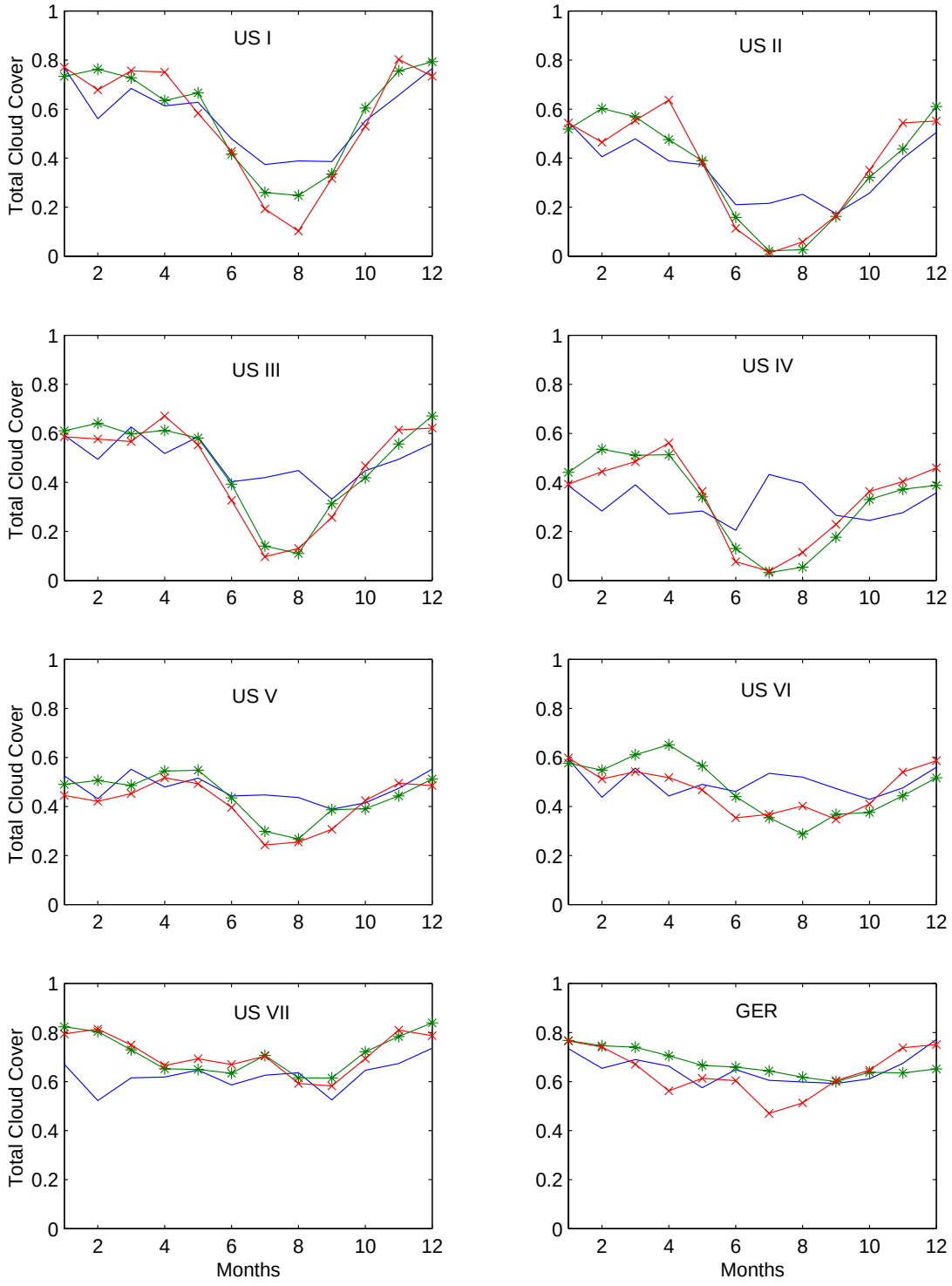

FIG. 7. The annual cycles of the total cloud cover amount for the eight regions as shown in figure 1b. The blue '__' line represents the observations, the green '*' the present−day "PD" and the red '+' the pre−industrial "PI" experiment.

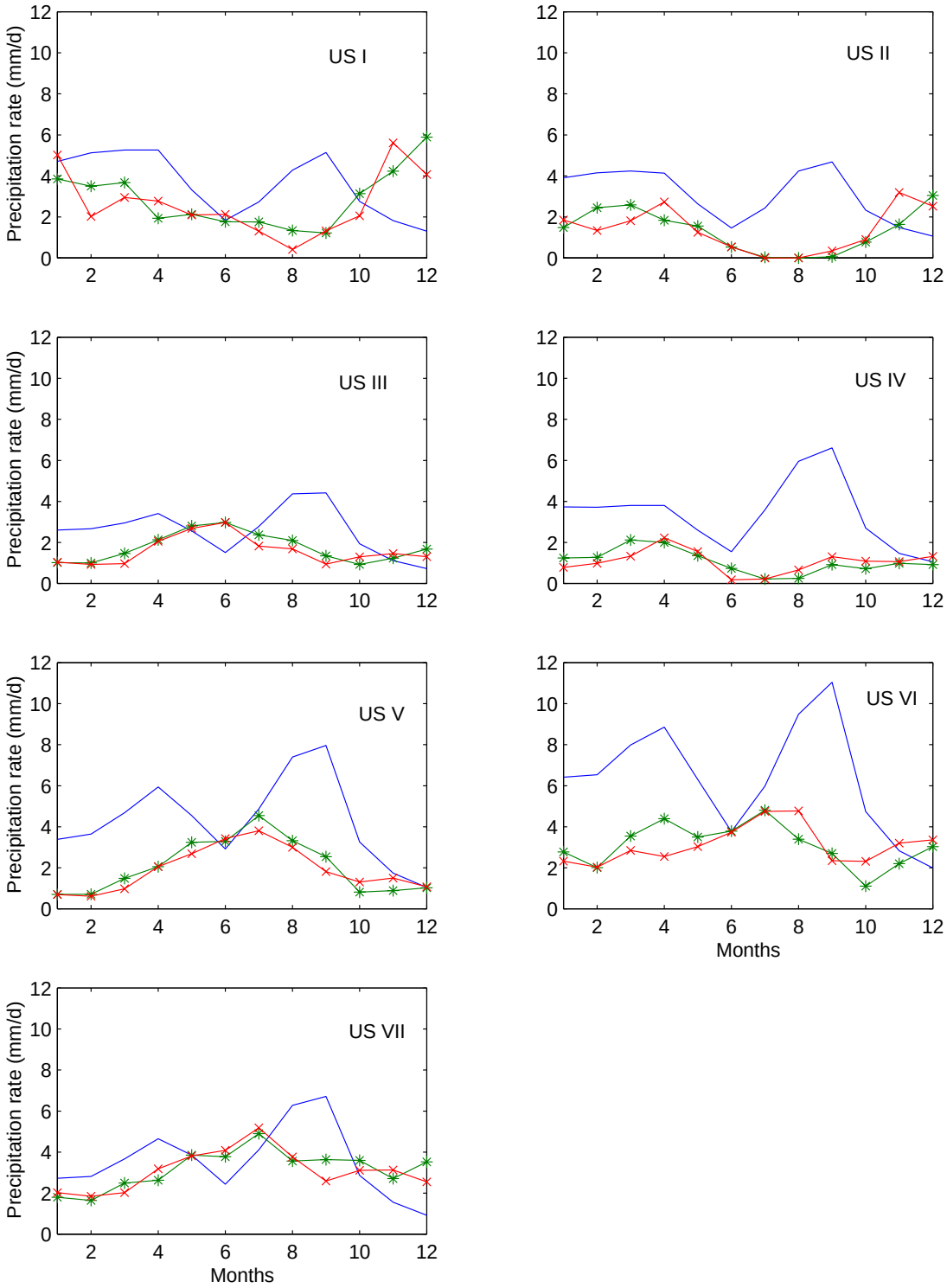

FIG. 8. The annual cycles of the precipitation rate for the eight regions as shown in figure 1b. The blue '__' line represents the observations, the green '*' the present−day "PD" and the red '+' the pre−industrial "PI" experiment.

Figure 7 shows the fractional cloud cover. The observed u−shaped seasonal distribution is correctly modeled by ECHAM4. Most striking, however, is the discrepancy between observed and modeled fractional cloud cover in the US boxes in summer. The modeled cloud cover is too low in summer, especially the continental boxes US II, US III and US IV, and slightly too high in winter in all US boxes. The more realistic aerosol load of the PD experiment does not seem to improve this feature substantially.

The observed distributions of the precipitation rates in figure 8 can be described as bi−modal curves for all regions. The minima are in June and December and the maxima occur in April and September. Whereas the modeled seasonal cycles are more sinus−like with the minima either in July, August for the boxes west of the Rocky Mountains USI, USII, USIV or in January, February for the central and eastern regions. The two model experiments itself are quite similar and differences are of secondary order.

It can be seen in figure 6, 7 and 8, that the all sky modeled solar irradiance follows the modeled fractional cloud cover very well. And the modeled precipitation cycles are either in phase (USI, USII, US IV) or out of phase (USIII, USV, USVI, USVII) with the modeled cloud cover cycles. This is in contrast to the observational precipitation, which is completely unrelated to the observed cloud cover in the regions studied here. The drop in cloud cover in July and August − below 0.1 cloud coverage for the continental boxes − is coupled with enhanced solar fluxes in the model and explains the overestimated solar irradiance for these months. The model overestimated cloud cover in winter compared to the observational data is also in agreement with the underestimation of the solar fluxes of the all sky category. This means, that with increasing distance from the ocean the model artificially amplifies the seasonal cycle of the solar irradiance and the cloud coverage.

The precipitation rate for June, the month of the observed maximum, is sufficiently well modeled. However, in the following months the cloud cover drops unrealistically (not the eastern boxes USVI and UVII) and the precipitation rates fall consequently instead of reaching the observed maximum in September. The excessive solar irradiance would force convection if enough water were stored and thus keep the hydrological cycle intact. Note that the observed September maximum in precipitation is never reached either on the Coast nor inland. Independent studies confirm this bias. For example Roeckner et al. (1996) show positive temperature anomalies of 3K over Western US in June, July, August when the ECHAM4−GCM was compared with the ECMWF reanalysis data. No significant bias in the zonal wind component could be detected, only a negative pressure anomaly of −5hPa over Western United States in summer.

The enhanced aerosol load of the present−day experiment does not notably improve this feature. Furthermore, the indirect aerosol effect is not always negative. For some boxes and certain months (April/May in the boxes US I, US II, US III, USIV, GER) the modeled solar irradiance of the pre−industrial experiment is lower than the present−day solar flux. The higher surface solar radiation in PD is almost always combined with lower cloud coverage and lower precipitation rates in PD. That means even an enhanced aerosol load in these months does not increase cloudiness in the model and in contrast it decreases cloudiness slightly. This seems to be a contradiction to the second indirect effect or Albrecht effect which states that increasing aerosol concentration increases CDNC, which slows down precipitation formation and leads to longer lifetimes of clouds and thus increasing cloudiness. The positive effect occurs only in months when the cloud cover is already the highest of the year and precipitation is also high. Subsequently increasing CDNC does not necessarily lead to increasing cloud coverage even when the

precipitation is suppressed. Note that the semi−direct aerosol effect is not accounted for in these experiments (non−absorbing aerosols). Only in Germany, during April, May and June is the higher solar irradiance of the present−day experiment coupled with higher fractional cloud cover (see figure 6 and 7). An enhanced formation of high−level clouds with declining low−level clouds can be seen in the modeled results (figure 9) for the box GER. This shift in altitude causes the increasing transmissivity, since cirrus clouds are optically thinner than low−level clouds. An increase in CDNC could lead to an increase in contact nucleation and therefore more ice clouds in the model. The fact that the present−day experiment fits better with the observations implies the plausibility of this effect. The globally averaged annual mean value of the ice water path, however, does not change significantly, according to Lohmann and Feichter (1997).

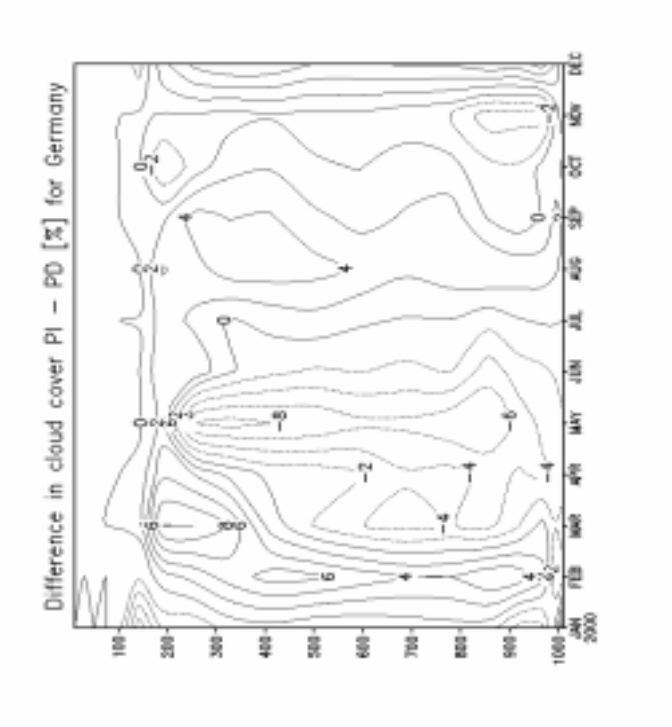

FIG. 9. Seasonal differences in cloud coverage with height for the German box GER between the two model experiments present−day PD and pre−industrial PI aerosol load.

8. Discussion

Surface climatologies of solar irradiance, fractional cloud cover and precipitation rates for the US and Germany are used to study the aerosol−cloud−interactions in the ECHAM4−GCM experiments (Lohmann and Feichter, 1997). The comparison of observational data with two model experiments reveal that the model predicts the annual mean cloud cover almost exactly as observed. However, the annual cycle is over−emphasized in all boxes especially in the inner continent of the United States. Prominent declines in the July and August monthly means of the fractional cloud coverage are

detected and, on the other hand, the winter cloud cover is always overestimated. The model experiment, which includes the indirect aerosol effect, improves this deficiency only slightly and the major differences remain. The annual cycle of the solar radiation reflects this erroneous cloud cover amplification.

We suspect that neither the cloud scheme nor the radiation code alone causes this amplification of the seasonal cycle. Rather, the relative humidity might be the dominant factor. Relative humidity may be underestimated in summer, when the model evaporation in the inner continent becomes too low and vice versa overestimated in winter, when modeled evaporation is too high. Deficiencies in leaf area index and vegetation ratio and/or soil moisture capacity may lead to the exaggerated hydrological cycle. Soil and vegetation parameters are annual mean values in the model. Wild et al. (1996) showed how soil moisture drops dramatically in the ECHAM3−GCM in late summer compared to observations at two Central European sites. The same process might be responsible for the deficiencies on the North− American continent. The seasonal variability of one vegetation or soil type may sometimes be of similar importance than the difference between various types itself.

The $+23 W/m^2$ underestimation of the modeled solar radiation under overcast conditions can also be explained with the lack of seasonality in the hydrological cycle. Overcast skies are mainly observed in the winter half of the year when the evaporation may be overestimated. The indirect aerosol effect only comes on top of these systematic deficiencies.

The observed seasonal cycle of the precipitation is not simulated correctly in all boxes. The spring and fall maximum of precipitation is not modeled at all. This discrepancy in the precipitation rate might at least partly be related to the surface conditions as well.

With the missing water storage, suppressed evaporation in summer may lead to fewer convective clouds and hence reduced convective precipitation. On the other hand, shower formation and convection is a sub−grid process and deficiencies in sub−grid precipitation formation itself could also cause these discrepancies. Improved formation of sub−grid precipitation in contrast to large− scale precipitation may lead to more realistic precipitation rates in the model.

However, coastal boxes are not as strongly affected by the land surface deficiencies as continental boxes. An example is the German box where the present−day experiment improves the seasonal cycle of the solar irradiance at the surface as compared to the pre−industrial experiment. Figure 10a and 10b show the overcast sky solar radiation for this box, which is clearly more realistic. The cloud cover distribution and the seasonal cycle also improves when compared to observations. The solar radiation and cloud cover comparisons between the two model experiments PI and PD indicate a possible shift to increasing occurrence of higher clouds in early summer due to the indirect aerosol effect. This result supports a former study published by the author (Liepert, 1997) in which a 13% increase in cirrus clouds over two German sites (Hamburg, Hohenheissenberg) were shown between 1964 and 1990. This increase was accompanied by a decline in diffuse solar radiation. Increasing air traffic and consequently increasing contrails alone were not responsible for this decline. Therefore, the indirect aerosol effect was suggested as possible reason. Another study from Parungo et al. (1994) showed a significant increasing trend in the globally averaged mid−level cloud coverage over the ocean from 1952 to1981. They suggested increasing anthropogenic sulfate aerosols in the free troposphere as a possible reason for the increase (see also comment from Norris and Leovy (1995) and the reply from Parungo (1995)).

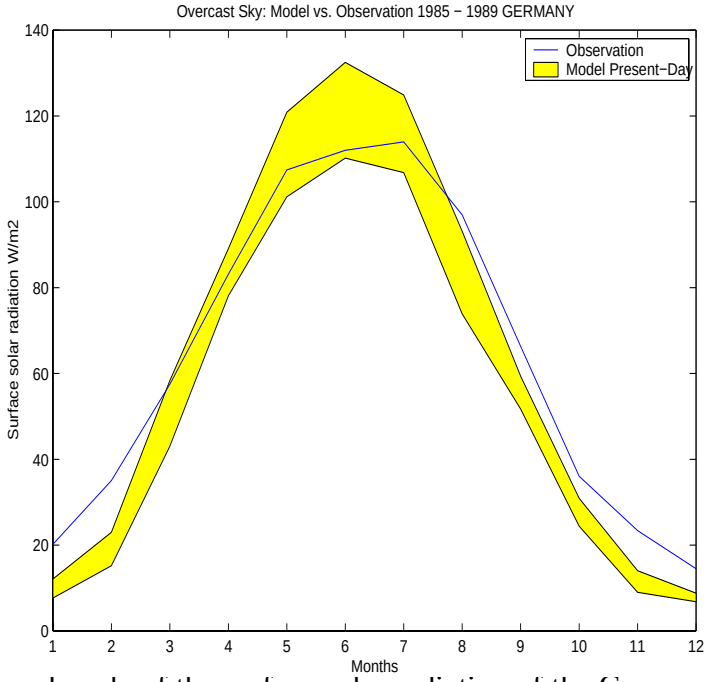

FIG. 10a. The annual cycle of the surface solar radiation of the German box for overcast sky and the pre−industrial "PI" experiment. The shaded area is the uncertainty range due to the selection criteria of overcast sky, which is defined as all data between 7/8 and 8/8 sky cover.

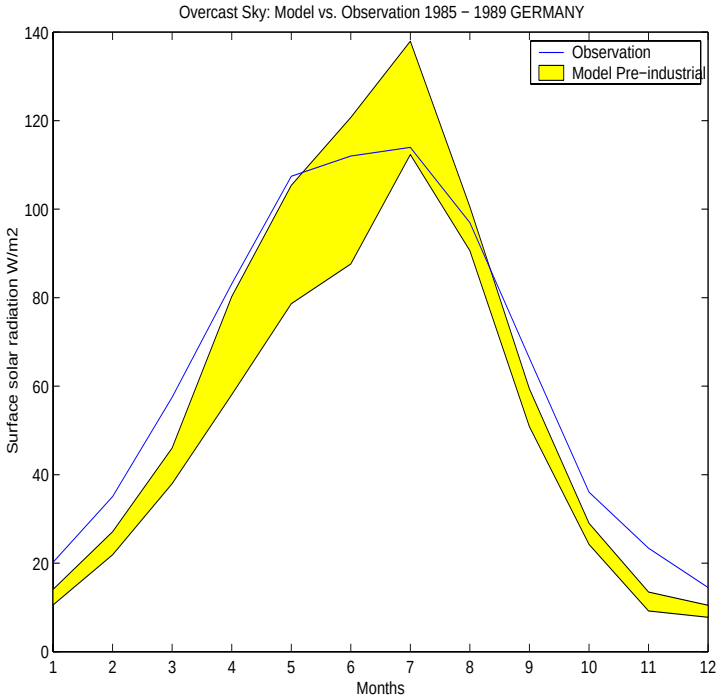

FIG. 10b. The annual cycle of the surface solar radiation of the German box for overcast sky and the present−day "PD" experiment. The shaded area is the uncertainty range due to the selection criteria of overcast sky, which is defined as all data between 7/8 and 8/8 of sky cover.

In summary, observed cloud cover variability over land is generally in agreement with the ECHAM4 GCM experiments used in this study. Annual means of solar irradiance and precipitation rates are underestimated. Comparisons of the observed and modeled climatologies reveal even some features of the indirect aerosol effect. However, model discrepancies, which most likely stem from other branches of the hydrological cycle − i.e. annually fixed vegetation ratio and soil moisture capacity − and not necessarily the cloud or radiation scheme itself obscure these features.

ACKNOWLEDGEMENTS

We would like to thank the reviewers for their comments and helpful suggestions. We also would like to thank the National Climate Data Center NCDC of the US Department of Commerce and the German Weather Service for providing the data. This work was sponsored by US Department of Energy Atmospheric Radiation Program ARM grant DE−FG02−97ER62393, NASA Global Aerosol Climatology Project GACP grant NAG 5−7687 and the National Sciences and Engineering Research Council of Canada.

REFERENCES

Boucher, O. and U. Lohmann, 1995: The sulfate−CCN−cloud albedo effect. *Tellus,* **47B**, 281−300.

Chuang, C. C., J. E. Penner, K. E. Taylor, A. S. Grossmann, and J. J. Walton, 1997: An assessment of the radiative effects of anthropogenic sulfate. *J. Geophys. Res.,* **102**, D3, 3761−3778.

Feichter, J., E. Kjellstroem, H. Rodhe, F. Dentener, J. Lelieveld, and G. J. Roelofs, 1996: Simulation of tropospheric sulfur cycle in a global climate model. *Atmos. Environ.,* **30**, 1693−1707.

Gates, W. L., 1992: AMIP: The atmospheric model intercomparison project. *Bull. Am. Meteorol. Soc.,* **73**, 1962−1970.

Jones, A., D. L. Roberts, and A. Slingo, 1994: A climate model study of radiative forcing by anthropogenic sulphate aerosols. *Nature,* **370**, 450−453.

Kogan, Z. N., Y. L. Kogan, and D. K. Lilly, 1996: Evaluation of sulfate aerosols indirect effect in maritime stratocumulus clouds using observation−derived cloud climatology. *Geophys. Res. Lett.,* **98**, 22,949−22,958.

Liepert, B. G. and G. J. Kukla, 1997: Decline in global solar radiation with increased horizontal visibility in Germany between 1964 and 1990. *J. Climate,* **10**, 2391−2401.

Liepert, B. G., 1997: Recent changes in solar radiation under cloudy conditions in Germany. *Int. J. Climatol.,* **17**, 1581−1593.

Lohmann, U. and E. Roeckner, 1996: Design and performance of a new cloud microphysics scheme developed for the ECHAM general circulation model. *Climate Dynamics,* **12**, 557−572.

Lohmann, U. and J. Feichter, 1997: Impact of sulfate aerosols on albedo and lifetime of clouds: a sensitivity study with the ECHAM4 GCM. *J. Geophys. Res.,* **102,** D12, 13,685−13,700.

NREL, 1992: User's manual: National Solar Radiation Database. Version 1.0, distributed by National Climate Data Center, Federal Building, Asheville, NC 28801, 93 pp.

Norris, J. R. and C. B. Leovy,1995: Comments on "Trends in global marine cloudiness and anthropogenic sulfur. *J. Climate,* **8**, 2109−2110.

Ohmura, A., E.G. Dutton, B. Forgan, C. Froehlich, H. Gilgen, H. Hegner, A. Heimo, G. Koenig−Langlo, B. McArthur, G. Mueller, R. Philipona, R. Pinker, C. Whitlock, K. Dehne, M. Wild, 1998: Baseline surface radiation network (BSRN/WCRP): New precision radiometry for climate research. *Bull. Amer. Meteor. Soc.*, **79/10**, 2115−2136.

Parungo, F., J. F. Boatman, H. Sievering, S. W. Wilkison, and B. B. Hicks, 1994: Trends in global marine cloudiness and anthropogenic sulfur. *J. Cimate,* **7**, 434−440.

Parungo, F., 1995: Reply. *J. Climate*, **8**, 2111−2112.

Roeckner, E., K. Arpe, L. Bengtsson, M. Christoph, M. Claussen, L. Duemenil, M. Esch, M. Giorgetta, U. Schlese, U. Schulzweida, 1996: The atmospheric general circulation model ECHAM−4: model description and simulation of present−day climate. Report 218 of the Max−Planck Institute for Meteorology, Hamburg Germany, 30pp.

Sundqvist, H., E. Berge, and J. E. Kristjansson, 1989: Condensation and cloud parameterization studies with mesoscale numerical weather prediction model. *Monthly Wea. Rev.*, **117**, 1641−1657.

Wild, M., L. Duemenil, and J.−P. Schulz, 1996: Regional climate simulation with a high resolution GCM: surface hydrology. *Climate Dynamics*, **12**, 755−774.

Wild, M. and B. Liepert, 1998: Excessive transmission of solar radiation through the cloud−free atmosphere in GCMs. *Geophys. Res. Lett.*, **25**, No.12, 2165−2168.